

1 **Ensemble Prediction of Air Quality Using the WRF/CMAQ Modeling System for Health**
2 **Effects Studies in China**

3
4 Jianlin Hu¹, Xun Li¹, Lin Huang¹, Qi Ying^{2,1}, Qiang Zhang³, Bin Zhao⁴, Shuxiao Wang⁴,
5 Hongliang Zhang^{5,1*}

6
7 ¹ Jiangsu Key Laboratory of Atmospheric Environment Monitoring and Pollution Control,
8 Jiangsu Engineering Technology Research Center of Environmental Cleaning Materials, Jiangsu
9 Collaborative Innovation Center of Atmospheric Environment and Equipment Technology,
10 School of Environmental Science and Engineering, Nanjing University of Information Science &
11 Technology, 219 Ningliu Road, Nanjing 210044, China

12 ² Zachry Department of Civil Engineering, Texas A&M University, College Station, TX 77843-
13 3136

14 ³ Ministry of Education Key Laboratory for Earth System Modeling, Center for Earth System
15 Science, Tsinghua University, Beijing, China

16 ⁴ State Key Joint Laboratory of Environment Simulation and Pollution Control, School of
17 Environment, Tsinghua University, Beijing 100084, China

18 ⁵ Department of Civil and Environmental Engineering, Louisiana State University, Baton Rouge,
19 LA 77803

20
21 *Corresponding author:

22 Hongliang Zhang, Email: hlzhang@lsu.edu. Phone: +1-225-578-0140.

23 **Abstract**

24
25 Accurate exposure estimates are required for health effects analyses of severe air pollution in
26 China. Chemical transport models (CTMs) are widely used to provide spatial distribution,
27 chemical composition, particle size fractions, and source origins of air pollutants. The accuracy
28 of air quality predictions in China is largely affected by the uncertainties of public available
29 emission inventories. The Community Multiscale Air Quality (CMAQ) model with
30 meteorological inputs from the Weather Research and Forecasting (WRF) model were used in
31 this study to simulate air pollutants in China in 2013. Four sets of simulations were conducted
32 with four different anthropogenic emission inventories, including the Multi-resolution Emission
33 Inventory for China (MEIC), the Emission Inventory for China by School of Environment at
34 Tsinghua University (SOE), the Emissions Database for Global Atmospheric Research
35 (EDGAR), and the Regional Emission inventory in Asia version 2 (REAS2). Model performance
36 was evaluated against available observation data from 422 sites in 60 cities across China. Model
37 predictions of O₃ and PM_{2.5} generally meet the model performance criteria, but performance
38 difference exists in different pollutants and regions among inventories. Ensemble predictions
39 were calculated by linearly combining the results from different inventories to minimize the sum
40 of the squared errors between the ensemble results and the observations from all the cities. The
41 ensemble concentrations show improved agreement with observations in most cities. The mean
42 fractional bias (MFB) and mean fractional errors (MFE) of the ensemble annual PM_{2.5} at the 60
43 cities are -0.11 and 0.24, respectively, which are better than the MFB (-0.25 – -0.16) and MFE
44 (0.26 – 0.31) of individual simulations. The ensemble annual daily maximum 1-hour O₃ (O₃-1h)
45 concentrations are also improved, with mean normalized bias (MNB) of 0.03 and mean
46 normalized errors (MNE) of 0.14, compared to MNB of 0.06 – 0.19 and MNE of 0.16 – 0.22 of
47 the individual predictions. The ensemble predictions agree better with observations with daily,
48 monthly, and annual averaging times in all regions of China for both PM_{2.5} and O₃-1h. The study
49 demonstrates that ensemble predictions by combining predictions from individual emission
50 inventories can improve the accuracy of predicted temporal and spatial distributions of air
51 pollutants. This study is the first ensemble model study in China using multiple emission
52 inventories and the results are publicly available for future health effects studies.

53
54 **Key words:** chemical transport model; emission inventory; ensemble; China; PM_{2.5}

55 1. Introduction

56
57 A significant portion of the population in China has been exposed to severe air pollution in
58 recent decades as the consequence of intensive energy use without efficient control measures.
59 Based on ambient air pollution data published by the China National Environmental Monitoring
60 Center (CNEMC), most of the major cities are in violation of the Chinese Ambient Air Quality
61 Standards grade II standard ($35 \mu\text{g m}^{-3}$) for annual average particulate matter with diameter of
62 $2.5 \mu\text{m}$ or less ($\text{PM}_{2.5}$) (Zhang and Cao, 2015; Wang et al., 2014b), with a mean population
63 weighted $\text{PM}_{2.5}$ concentration of over $60 \mu\text{g m}^{-3}$ during 2013-2014. Long-term exposure to such
64 high levels of $\text{PM}_{2.5}$ greatly threatens public health in China. Recent studies have suggested that
65 approximately more than one million premature deaths can be attributed to outdoor air pollution
66 each year in China (Lelieveld et al., 2015a; Liu et al., 2016; Hu et al., 2017a).

67
68 Accurate exposure estimates are required in health effects studies. Ambient air quality is usually
69 measured at monitoring sites and used to represent the exposure of population in the surrounding
70 areas. However, a routine central monitoring network in China has just been established since
71 2013, and is still limited in spatial coverage and lack of detailed information of the chemical
72 composition, PM size fractions, and source origins of air pollutants. Chemical transport models
73 (CTMs) have been widely used in health effects studies to overcome the limitations in central
74 monitor measurements for exposure estimates (Philip et al., 2014; Lelieveld et al., 2015b; Liu et
75 al., 2016; Laurent et al., 2016a; Laurent et al., 2016b; Ostro et al., 2015). However, the accuracy of
76 the predictions from CTMs is largely affected by the accuracies of the emission inventories
77 (Wang et al., 2010), meteorological fields (Hu et al., 2010), and numerical solutions to the
78 equations that describe various atmospheric processes (Hu et al., 2006; Yu et al., 2005). Emission
79 inventories are indispensable tools for a wide range of environmental activities from
80 management of chemicals to the prevention of air pollution. Several emission inventories have
81 been created to cover China. Different emission inventories focus on specific geographical
82 regions in the urban, regional (Zhao et al., 2012; Zhang et al., 2008), national or continental
83 (Zhang et al., 2009; Kurokawa et al., 2013) scales; and/or focus on pollutants from individual (Su
84 et al., 2011; Ou et al., 2015) and specific sectors (Zhao et al., 2008; Xu et al., 2017).

85
86 Despite the great efforts in improving the accuracy of emission inventories in China, large
87 uncertainties still remain. Generally, the emissions of pollutants are estimated as the product of
88 activity levels (such as industrial production or energy consumption), unabated emission factors
89 (i.e. mass of emitted pollutant per unit activity level), and the efficiency of emission controls.
90 Large uncertainties are associated with activity levels, emission source fractions, and emission
91 factors (Akimoto et al., 2006; Lei et al., 2011a). The uncertainties are especially significant for
92 some pollutants, such as ammonia (NH_3) and volatile organic compounds (VOCs). For example,
93 for a Pearl River Delta (PRD) inventory in 2006, SO_2 emission has low uncertainties of -
94 16%~21% from power plant sources quantified by Monte Carlo simulations, while NO_x has
95 medium to high uncertainties of -55%~150% and VOC, CO, and PM have even higher
96 uncertainties (Zheng et al., 2009). For an inventory for the Yangtze River Delta (YRD) region,
97 the overall uncertainties for CO, SO_2 , NO_x , PM_{10} , $\text{PM}_{2.5}$, VOCs, and NH_3 emissions are $\pm 47.1\%$,
98 $\pm 19.1\%$, $\pm 27.7\%$, $\pm 117.4\%$, $\pm 167.6\%$, $\pm 133.4\%$, and $\pm 112.8\%$, respectively (Huang et al.,
99 2011). A comprehensive quantification study by Zhao et al. (2011) using Monte Carlo
100 simulations showed that the uncertainties of Chinese emissions of SO_2 , NO_x , $\text{PM}_{2.5}$, BC, and OC

101 in 2005 are -14%~13%, -13%~37%, -17%~54%, -25%~136%, and -40%~121%,
102 respectively.

103
104 The uncertainties in emission inventories are carried into CTMs simulations, leading to biases in
105 air quality predictions, which need to be carefully evaluated to identify the useful information for
106 health effects studies (Hu et al., 2016b;Hu et al., 2014c;Hu et al., 2014b;Hu et al., 2015b;Tao et
107 al., 2014). An evaluation of one-year air pollutants predictions using the Weather Research and
108 Forecasting (WRF) / Community Multi-scale Air Quality (CMAQ) modeling system with the
109 Multi-resolution Emission Inventory for China (MEIC) has been reported (Hu et al., 2016a). The
110 model predictions of O₃ and PM_{2.5} generally agree with ambient measured concentrations, but
111 the model performance varies in different regions and seasons. In some regions, such as the
112 northwest of China, the model significantly under-predicted PM_{2.5} concentrations.

113
114 The technique of ensemble is often used to reduce uncertainties in model predictions by
115 combining multiple sets of predictions. This technique has been widely used in the climate
116 predictions (Murphy et al., 2004;Tebaldi and Knutti, 2007), and recently adopted in air quality
117 predictions (Delle Monache et al., 2006;Huijnen et al., 2010). A recent study has compared a few
118 anthropogenic emission inventories in China during 2000-2008 (Saikawa et al., 2016), but
119 detailed evaluation of model results based on these inventories have not been performed. The
120 methods to utilize the strength of different emission inventories to get improved air quality
121 predictions for China have not been reported in the literature. The aim of this study is to create
122 an improved set of air quality predictions in China by using an ensemble technique. First, four
123 sets of one-year air quality predictions were conducted with the WRF/CMAQ modeling system
124 with four different anthropogenic emission inventories for China in 2013. In addition to MEIC,
125 the three other emission inventories are the Emissions Database for Global Atmospheric
126 Research (EDGAR), Regional Emission inventory in Asia version 2 (REAS2), and Emission
127 Inventory for China developed by School of Environment at Tsinghua University (SOE). The
128 model performance on PM_{2.5} and O₃ concentrations in 2013 with different emission inventories
129 was then evaluated against available observation data in 60 cities in China. The differences
130 among air quality predictions were also compared and identified. Finally, an ensemble technique
131 was developed to minimize the bias of model predictions and to create improved exposure
132 predictions. To the authors' best knowledge, this is the first ensemble model study in China
133 using multiple emission inventories. The ensemble predictions of this study are available for
134 public health effects analyses.

135
136 This paper is organized as follows. The CMAQ model, emissions and other inputs for the model,
137 observational datasets used for model performance evaluation, and the method for ensemble
138 calculation are described in Section 2. Section 3 discusses the model performance on gaseous
139 and particulate pollutants simulated with four emission inventories, as well as the performance of
140 the ensemble predictions in different regions/cities and with different averaging times. At last,
141 the major findings are summarized in the Conclusion section.

142 **2. Method**

143 **2.1 Model description**

144

145 In this study, the applied CMAQ model is based on CMAQ v5.0.1 with changes to improve the
146 model's performance in predicting secondary organic and inorganic aerosols. The details of these
147 changes could be found in previous studies (Hu et al., 2016a;Hu et al., 2017b) and the
148 references therein, therefore only a brief description is summarized here. The gas phase
149 photochemical mechanism SARPC-11 was modified to better treat isoprene oxidation chemistry
150 (Ying et al., 2015;Hu et al., 2017b). Formation of secondary organic aerosol (SOA) from
151 reactive uptake of dicarbonyls, methacrylic acid epoxide, and isoprene epoxydiol through surface
152 pathway (Li et al., 2015;Ying et al., 2015) was added. Corrected SOA yields due to vapor wall-
153 loss (Zhang et al., 2014) were adopted. Formation of secondary nitrate and sulfate through
154 heterogeneous reactions of NO₂ and SO₂ on particle surface (Ying et al., 2014) was also
155 incorporated. It has been shown that these modifications improved the model performance on
156 secondary inorganic and organic PM_{2.5} components.
157

158 **2.2 Anthropogenic emissions**

159
160 The CMAQ model was applied to China and surrounding countries in East Asia using the
161 horizontal resolution of 36-km. The modeling domain is shown in Figure 1. The anthropogenic
162 emissions are from four inventories: MEIC, SOE, EDGAR, and REAS2. MEIC was developed
163 by a research group in Tsinghua University (<http://www.meicmodel.org>). Compared with other
164 inventories for China, e.g. INTEX-B (Zhang et al., 2009) or TRACE-P (Streets et al., 2003), the
165 major improvements include a unit-based inventory for power plants (Wang et al., 2012) and
166 cement plants (Lei et al., 2011b), a county-level high-resolution vehicle inventory (Zheng et al.,
167 2014), and a novel NMVOC speciation approach (Li et al., 2014). The VOCs were speciated to
168 the SAPRC-07 mechanism. As the detailed species to model species mapping of the SAPRC-11
169 mechanism is essentially the same as the SAPRC-07 mechanism (Carter and Heo, 2012), the
170 speciated VOC emissions in the MEIC inventory were directly used in the simulation.
171

172 The SOE emission inventory was developed using an emission factor method (Wang et al.,
173 2011;Zhao et al., 2013). The sectorial emissions in different provinces were calculated based on
174 activity data, technology-based and uncontrolled emissions factors, and penetrations (fractions of
175 pollutants not collected) of control technologies. Elemental carbon (EC) and organic carbon
176 (OC) emissions were calculated based on PM_{2.5} emissions and their ratios to PM_{2.5}. The sectorial
177 activity data and technology distribution were obtained using an energy demand modeling
178 approach with various Chinese statistics and technology reports. More details, including the
179 spatio-temporal distributions and speciation of NMVOC emissions, can be found in previous
180 publications (Zhao et al., 2013;Wang et al., 2011;Bin et al., 2013). Since MEIC and SOE
181 emission inventories only cover China, emissions from outside China countries and regions were
182 based on REAS2 (Kurokawa et al., 2013).
183

184 The version 4.2 of EDGAR emission (<http://edgar.jrc.ec.europa.eu/overview.php?v=42>) has a
185 spatial resolution of 0.1°×0.1°. The EDGAR inventory contains annual emissions from different
186 sectors based on IPCC designations. REAS2 has a spatial resolution of 0.25° ×0.25° for the entire
187 Asia. The inventory contains monthly emissions of pollutants from different source categories.
188 Saikawa et al. (2016) compared the major features of different anthropogenic emission
189 inventories for China. Detailed information regarding these inventories can be found in the
190 publications presenting them. Table S1 shows the total emissions of major pollutants within

191 China in a typical workday of each season. In general, large differences exist among different
192 inventories for China. MEIC has the highest CO emissions in winter while REAS2 has the
193 highest in other seasons. MEIC has the highest NO_x emissions while REAS2 has the highest
194 emissions of VOCs in all seasons. EDGAR predicts the highest SO₂ emissions, which are
195 approximately a factor of two higher than those estimated by SOE. SOE has highest NH₃
196 emissions while EDGAR has much lower NH₃ emissions than the other three. EDGAR also has
197 lowest EC and OC emissions, but the total PM_{2.5} emissions are the highest. Standard deviations
198 indicate that winter has the largest uncertainties for all species except SO₂ and NH₃. Winter has
199 the smallest SO₂ uncertainties while summer has the largest NH₃ uncertainties.

200
201 All the emissions inventories were processed with an in-house program and re-gridded into the
202 36-km resolution CMAQ domain when necessary. Representative speciation profiles based on
203 the SPECIATE 4.3 database maintained by U.S. EPA were applied to split NMVOC of EDGAR
204 and REAS2 into SAPRC-11 mechanism and PM_{2.5} of all inventories was split into AERO6
205 species. Monthly emissions were temporally allocated into hourly files using temporal allocation
206 profiles from previous studies (Chinkin et al., 2003; Olivier et al., 2003; Wang et al., 2010a).
207 More details regarding EDGAR can be found in Wang et al. (2014a), while those for REAS2 can
208 be found in Qiao et al. (2015).

210 **2.3 Other inputs**

211
212 The Model for Emissions of Gases and Aerosols from Nature (MEGAN) v2.1 was used to
213 generated biogenic emissions (Guenther et al., 2012). The 8-day Moderate Resolution Imaging
214 Spectroradiometer (MODIS) leaf area index (LAI) product (MOD15A2) and the plant function
215 type (PFT) files used in the Global Community Land Model (CLM 3.0) were applied to generate
216 inputs to MEGAN. The readers are referred to Qiao et al. (2015) for more information. Open
217 biomass burning emissions were generated using a satellite observation based fire inventory
218 developed by NCAR (Wiedinmyer et al., 2011). The dust emission module was updated to be
219 compatible with the 20-category MODIS land use data (Hu et al., 2015a) for in-line dust
220 emission processing and sea salt emissions were also generated during CMAQ simulations.

221
222 The meteorological inputs were generated using WRF v3.6.1 (Skamarock et al., 2008). The
223 initial and boundary conditions to WRF were downloaded from the NCEP FNL Operational
224 Model Global Tropospheric Analyses dataset. WRF configurations details can be found in Zhang
225 et al. (2012). WRF performance has been evaluated by comparing predicted 2m above surface
226 temperature and relative humidity, and 10m wind speed and wind direction with all available
227 observational data at ~1200 stations from the National Climate Data Center (NCDC). The model
228 performance is generally acceptable and detailed evaluation results can be found in a previous
229 study (Hu et al., 2016a).

230
231 The initial and boundary conditions representing relatively clean tropospheric concentrations
232 were generated using CMAQ default profiles.

234 **2.4 Model evaluation**

235

236 Model predictions with the four emission inventories were evaluated against available
 237 observation data in China. Hourly observations of PM_{2.5}, PM₁₀, O₃, CO, SO₂, and NO₂ from
 238 March to December 2013 at 422 stations in 60 cities were obtained from CNEMC
 239 (<http://113.108.142.147:20035/emcpublish/>) but no observations were available for January and
 240 February. Observations at multiple sites in one city were averaged to calculate the average
 241 concentrations of the city. Detailed quality control of the data can be found in previous studies
 242 (Hu et al., 2016a; Hu et al., 2014a; Wang et al., 2014b). Statistical matrix of mean normalized bias
 243 (MNB), mean normalized error (MNE), mean fractional bias (MFB) and mean fractional error
 244 (MFE) were calculated using the Equations (E1)-(E4):
 245

$$246 \quad MNB = \frac{1}{N} \sum_{i=1}^N \left(\frac{C_m - C_o}{C_o} \right) \quad (E1)$$

$$247 \quad MNE = \frac{1}{N} \sum_{i=1}^N \left| \frac{C_m - C_o}{C_o} \right| \quad (E2)$$

$$248 \quad MFB = \frac{1}{N} \sum_{i=1}^N \left(\frac{C_m - C_o}{\frac{C_o + C_m}{2}} \right) \quad (E3)$$

$$249 \quad MFE = \frac{1}{N} \sum_{i=1}^N \left| \frac{C_m - C_o}{\frac{C_o + C_m}{2}} \right| \quad (E4)$$

250 where C_m and C_o are the predicted and observed city average concentrations, respectively, and
 251 N is the total number of observation data. MNB and MNE are commonly used in evaluation of
 252 model performance of O₃, and MFB and MFE are commonly used in evaluation of model
 253 performance of PM_{2.5} (Tao et al., 2014). The U.S. EPA previously recommended O₃ model
 254 performance criteria of within ± 0.15 for MNB and less than 0.30 for MNE (as shown in Figure 1)
 255 and PM model performance criteria of within ± 0.60 for MFB and less than 0.75 for MFE (EPA,
 256 2001b). Figure 2 includes the criteria and goals for PM as a function of PM concentration, as
 257 suggested by Boylan and Russell (2006), which have been widely used in model evaluation.
 258

259 2.5 Ensemble predictions

260
 261 The four sets of predictions with different inventories were combined linearly to calculate the
 262 ensemble predictions, as shown in Equation (E5):

$$263 \quad C^{pred,ens} = \sum_{m=1}^{N_m} w_m C^{pred,m} \quad (E5)$$

264 where $C^{pred,ens}$ is the ensemble prediction, $C^{pred,m}$ is the predicted concentration from the mth
 265 simulation, N_m is the number of simulations in the ensemble ($N_m=4$), and w_m is the weighting
 266 factor of the mth simulation. The weighting factor for each set of predictions was determined by
 267 minimizing the objective function Q in Equation (6):
 268

$$Q = \sum_i^{N_{city}} \left[C_i^{obs} - \sum_{m=1}^{N_m} w_m C_i^{pred,m} \right]^2 \quad (E6)$$

269 where C_i^{obs} is the observed PM_{2.5} or O₃ concentration at the i^{th} city, N_{city} is the total number of
 270 cities with observation (N=60), $C_i^{pred,m}$ is the predicted concentration at the i^{th} city from the m^{th}
 271 simulation, and N_m is the number of simulations in the ensemble ($N_m=4$). The weight factor w_m
 272 of the m^{th} simulation to be determined is within the range of [0, 1], with $w=0$ represents no
 273 influence of the individual simulation on the ensemble prediction, and $w=1$ indicates that
 274 concentrations of the individual simulation are fully accounted in the ensemble prediction. The
 275 observations data were the same as used in the model evaluation. Ensemble predictions were
 276 performed for PM_{2.5} and O₃ in this study. A MATLAB program was developed to solve above
 277 equation and determine the weighting factors using the linear least square solver “lsqin”.

278 279 3. Results

280 3.1 Model performance on gaseous and particulate pollutants

281 Table 1 summarizes the overall model performance on O₃, CO, NO₂, SO₂, PM_{2.5}, and PM₁₀ with
 282 different inventories using the averaged observations in 60 cities in 2013. Model performance
 283 meets the O₃ criteria for all inventories. O₃ from SOE are 7.2 parts per billion (ppb) lower than
 284 the mean observed concentration while the under-predictions of the other three inventories are
 285 less than 2 ppb. CO, NO₂, and SO₂ are under-predicted by all inventories, indicating potential
 286 uncertainties in the inventories. CO predictions from three inventories (SOE inventory does not
 287 include CO) are substantially lower than observations, with the best performance (lowest MNB
 288 and MNE) from REAS2. NO₂ overall performance is similar to CO. However, MEIC and SOE
 289 yield the lowest MNB, and EDGAR yields the highest. SO₂ performance is better than CO and
 290 NO₂, and MEIC and SOE yield the lowest MNB, while MNE values of the four inventories are
 291 very similar. PM_{2.5} and PM₁₀ predictions using all inventories meet the performance criteria with
 292 similar MFB and MFE values. REAS2 generally yields slightly better PM_{2.5} and PM₁₀
 293 performance, but all inventories under-predict the concentrations generally.

294 The difference in model performance with the four inventories also varies seasonally and
 295 spatially. Figure 2 shows the comparison of model performance for hourly gaseous species (O₃,
 296 CO, NO₂, and SO₂) in each month from March to December 2013. The MNB values of O₃ in
 297 most months are within the criteria for all inventories except for SOE, which under-predicts O₃
 298 concentrations. March has the worst performance for all inventories with MNE values larger than
 299 0.4 for MEIC, SOE, and EDGAR. No significant performance difference among different
 300 inventories in different months is found, but large difference exists in various regions of China
 301 (see the definition of regions of China in Figure 1). O₃ predicted using MEIC, EDGAR, and
 302 REAS2 meets the performance criteria in most regions except for YRD by MEIC and PRD by
 303 EDGAR. O₃ predicted using SOE only meets the criteria in Northwest (NW) and other region
 304 (Other) of China. CO and NO₂ are under-predicted in all regions, with the largest under-
 305 predictions in NW and Other. This pattern is similar among the results with all inventories. SO₂
 306 is generally under-predicted in all regions except, but over-predicted in the Sichuan Basin (SCB)
 307 by all inventories. SO₂ is also over-predicted by EDGAR in the PRD region. SO₂ in Northeast
 308 (NE) is substantially under-predicted by MEIC and REAS2. In general, model performance in
 309
 310

311 the more developed regions such as YRD, NCP, and PRD are relatively better, compared to NW
312 and Other regions.

313
314 Figure 3 illustrates the PM_{2.5} and PM₁₀ performance statistics of MFB and MFE as a function of
315 absolute concentrations in different months of 2013 and in different regions. PM_{2.5} predictions
316 based on each inventory are within the performance goal of MFB and between the goal and
317 criteria of MFE in all months. There is no significant difference among inventories. Half of
318 monthly averaged PM₁₀ MFB values fall within the goal while the rest are between the goal and
319 criteria. MFE values of PM₁₀ are all between the goal and criteria. From the regional perspective,
320 PM_{2.5} performance in NE by SOE is out of the MFB criteria, while that in SCB by MEIC, SOE,
321 and REAS2 are out of the MFE criteria. MFB values of PM₁₀ at all regions meet the criteria
322 except NW, due to under-estimation of windblown dust emissions in NW.

323

324 **3.2 Spatial variations in predicted gaseous and particulate pollutants**

325

326 Figure 4 shows the spatial distribution of annual averaged gas species, daily maximum 1-hour O₃
327 (O₃-1h), and 8-hour mean O₃ (O₃-8h), NO₂, and SO₂ predicted by MEIC and differences between
328 SOE, EDGAR, and REAS2 to MEIC. MEIC predicts annual O₃-1h concentrations are ~60ppb in
329 most parts of China with the highest values of ~70ppb in SCB. SOE predicts lower O₃-1h values
330 than MEIC, with about 5 ppb differences in the SCB, central China (CNT), and North China
331 Plain (NCP) regions and 2-3 ppb differences in other regions. EDGAR also predicts 2-3 ppb
332 lower O₃-1h in most regions than MEIC but its O₃-1h predictions in the Tibet Plateau, NCP and
333 ocean regions are 2-3 ppb higher than MEIC predictions. REAS2 predicted O₃-1h values are
334 lower than MEIC for scattered areas in the NE, NW, and CNT regions and other regions
335 experience slightly higher O₃-1h. MEIC, SOE, and REAS2 have similar results out of China (the
336 difference is generally less than 1 ppb) since the simulations used same emissions for those
337 regions. O₃-8h shows similar spatial distributions as O₃-1h among inventories with slightly less
338 differences. NO₂ concentrations are 10-15ppb in developed areas of the NCP and YRD regions,
339 and greater than 5 ppb at other urban areas as predicted by MEIC. SOE predicts 2-3 ppb lower
340 NO₂ concentrations in most areas except the vast NW region. EDGAR predicts lower NO₂ (more
341 than 5 ppb difference) in urban areas of the NCP and YRD areas but higher concentrations in the
342 entire west part of China by approximately 1-2 ppb. REAS2 has the closest NO₂ with MEIC as
343 the 1-2 ppb underestimation and overestimation are almost evenly distributed in the whole
344 country. SO₂ concentrations are up to 20ppb in the NCP, CNT, and SCB regions while are less
345 than 5 ppb in other regions. SOE mostly predicts 2-3 ppb lower SO₂ in the east half of China
346 with the largest difference of -10 ppb in the CNT region. EDGAR and REAS2 had very similar
347 difference with MEIC, i.e., more than 5 ppb higher concentrations in the NCP and YRD, ~2 ppb
348 higher concentrations in the PRD, 2-3 ppb lower concentrations in the NE and up to 5 ppb lower
349 concentrations in the CEN and SCB.

350

351 Figure 5 shows the seasonal distribution of PM_{2.5} total mass predicted by MEIC and differences
352 between SOE, EDGAR, and REAS2 to MEIC. In spring, MEIC predicted PM_{2.5} concentrations
353 are ~50 μg m⁻³ in east and south parts of China, and Southeast Asia has the highest value of ~100
354 μg m⁻³. SOE predicts 5-10 μg m⁻³ lower PM_{2.5} in north China and < 5 μg m⁻³ higher values in
355 south China and along the coastline. EDGAR predicts >20 μg m⁻³ lower values in NCP and ~10
356 μg m⁻³ lower values in NE, CNT, and SCB, but up to 20 μg m⁻³ higher values in PRD. REAS2

357 predicts higher $PM_{2.5}$ values in most parts of China except under-predictions in NE and SCB.
358 The over-predictions in YRD and NCP are up to $20\text{-}30\ \mu\text{g m}^{-3}$. In summer, the high $PM_{2.5}$
359 regions are much smaller compared to spring with $\sim 50\ \mu\text{g m}^{-3}$ ppb concentrations in NCP, north
360 part of YRD and SCB and $20\text{-}30\ \mu\text{g m}^{-3}$ in other parts. Generally, SOE predicts $<10\ \mu\text{g m}^{-3}$
361 lower values in most regions. EDGAR predicts lower values in NCP and SCB and $5\text{-}10\ \mu\text{g m}^{-3}$
362 higher values in south part. REAS2 almost predicts higher values in all the regions except some
363 scattered areas in NCP, YRD, and SCB.

364

365 In fall, $PM_{2.5}$ concentrations are larger than $50\ \mu\text{g m}^{-3}$ in most regions except NW and are ~ 100
366 $\mu\text{g m}^{-3}$ in part of NCP, CNT, and SCB. SOE predicted values are lower in north part and higher
367 in south part. EDGAR predicts up to $30\ \mu\text{g m}^{-3}$ lower values in NCP and SCB while up to $20\ \mu\text{g}$
368 m^{-3} higher values in YRD. REAS2 again estimates close values to MEIC with less than $5\ \mu\text{g m}^{-3}$
369 differences in most regions and up to $20\ \mu\text{g m}^{-3}$ higher values in scattered areas in YRD and SCB.
370 In winter, MEIC predicted $PM_{2.5}$ concentrations are up to $200\ \mu\text{g m}^{-3}$ in NCP, CNT, YRD, and
371 SCB, while PRD has concentrations of $\sim 50\ \mu\text{g m}^{-3}$. SOE severely underestimates by $30\ \mu\text{g m}^{-3}$ in
372 all regions with high $PM_{2.5}$ concentrations and only coast areas experience $<10\ \mu\text{g m}^{-3}$ higher
373 values. EDGAR also predicts $30\ \mu\text{g m}^{-3}$ lower $PM_{2.5}$ concentrations in NE, NCP, CNT, and SCB,
374 but the YRD region has $20\ \mu\text{g m}^{-3}$ higher values. The regions with lower values by REAS2
375 compared to MEIC are at the regions of NE, NCP, CNT and SCB, similar to EDGAR but with
376 much smaller areas. SOE predicts higher $PM_{2.5}$ in the south parts of YRD and NCP than MEIC.

377

378 Figure 6 shows the annual averaged concentrations of $PM_{2.5}$ components predicted by MEIC and
379 the differences between other inventories with MEIC. Annual averaged particulate sulfate (SO_4^{2-})
380 concentrations are $20\text{-}25\ \mu\text{g m}^{-3}$ in NCP, CNT, and SCB, and about $10\ \mu\text{g m}^{-3}$ in other regions in
381 the southeast China. SOE predicts $\sim 10\ \mu\text{g m}^{-3}$ lower values in high concentration areas and $2\text{-}3$
382 $\mu\text{g m}^{-3}$ lower in other areas. EDGAR predicts $\sim 5\ \mu\text{g m}^{-3}$ higher SO_4^{2-} in southeast China and $2\text{-}3$
383 $\mu\text{g m}^{-3}$ lower values in SCB. REAS2 predicted SO_4^{2-} are generally $2\text{-}3\ \mu\text{g m}^{-3}$ lower than that of
384 MEIC in areas except the coastal areas. MEIC predicts the highest particulate nitrate (NO_3^-)
385 concentrations of up to $30\ \mu\text{g m}^{-3}$ in NCP and YRD and values in other regions are $5\text{-}10\ \mu\text{g m}^{-3}$
386 except the northwest China. SOE predicts $<5\ \mu\text{g m}^{-3}$ lower values in the high concentrations
387 areas and $\sim 2\ \mu\text{g m}^{-3}$ higher values in coastal areas. EDGAR uniformly predicts lower NO_3^-
388 values than MEIC with the largest different of $10\ \mu\text{g m}^{-3}$. REAS2 has similar results to SOE.
389 Particulate ammonium (NH_4^+) concentrations predicted by MEIC have a peak of $15\ \mu\text{g m}^{-3}$ and
390 are mostly less than $10\ \mu\text{g m}^{-3}$ in the east and south parts of China. SOE predicts slightly lower
391 values except for coastal areas in PRD, where $1\text{-}2\ \mu\text{g m}^{-3}$ higher values are observed.

392

393 EC concentrations are generally low compared to other components as predicted by MEIC. The
394 highest values are less than $10\ \mu\text{g m}^{-3}$ in NCP, CNT and SCB. All other three inventories predict
395 $1\text{-}2\ \mu\text{g m}^{-3}$ lower EC values throughout the country. Primary organic aerosol (POA) predicted by
396 MEIC are $20\text{-}30\ \mu\text{g m}^{-3}$ in NCP, CNT and SCB, and are $\sim 10\ \mu\text{g m}^{-3}$ in other areas in east and
397 south parts of China. SOE predicts up to $5\ \mu\text{g m}^{-3}$ higher values in most areas with scattered
398 places with $\sim 2\ \mu\text{g m}^{-3}$ lower values compared to MEIC. EDGAR and REAS2 predict up to ~ 10
399 $\mu\text{g m}^{-3}$ lower values except for coastal areas. SOA concentrations are low in north part of China
400 and up to $10\ \mu\text{g m}^{-3}$ in the whole east and south parts. All three other inventories predict $\sim 2\ \mu\text{g}$
401 m^{-3} lower SOA values compared to MEIC. For other implicit components (OTHER), the highest
402 concentrations are $\sim 15\ \mu\text{g m}^{-3}$ in NW and NCP, while other regions have lower than $5\ \mu\text{g m}^{-3}$

403 concentrations. In NW, the major sources of OTHER are windblown dust online generated by
404 CMAQ simulations, thus almost no differences are observed among inventories. SOE and
405 EDGAR predict lower OTHER values in north part ($\sim 2 \mu\text{g m}^{-3}$) and slightly higher values in south
406 and east parts ($\sim 5 \mu\text{g m}^{-3}$). REAS2 predicts higher OTHER values in the whole east part
407 uniformly with up to $10 \mu\text{g m}^{-3}$ differences in NCP, YRD, and SCB regions.
408

409 Additional comparisons of model predictions in different regions and some major cities in China
410 are shown in Figures S1-S4 in the Supplemental Material.
411

412 3.3 Ensemble predictions

413
414 Above analyses indicate that model performance with different inventories varies on different
415 pollutants and in different regions. Table S2 shows the observed annual average concentrations
416 of $\text{PM}_{2.5}$ in the 60 cities and the predictions from the four inventories as well as the weighted
417 ensemble predictions. The weighting factors for predictions using MEIC, REAS2, SOE and
418 EDGAR are 0.31, 0.36, 0.24 and 0.20, respectively (Table 2). The ensemble predictions greatly
419 reduce MFB with a value of -0.11, compared to the MFB values of -0.25 – -0.16 using the annual
420 average concentrations in the individual simulations. Also, the ensemble predictions have an
421 MFE value of 0.24, lower than any MFE values of 0.26 – 0.31 in individual simulations (Figure
422 7). The ensemble predictions of annual O_3 -1h have the MNB and MNE of 0.03 and 0.14,
423 improved from MNB of 0.06 – 0.19 and MNE of 0.16 – 0.22 in the individual predictions,
424 respectively.
425

426 To further evaluate the ability of the ensemble method in improving predictions at locations
427 where observational data are not available, ensemble predictions were made using a data
428 withholding method. For each city, the observations at the other 59 cities were used to determine
429 the weighting factors in E6 and the ensemble prediction at the city was calculated. Performance
430 of the ensemble predictions at the city was calculated using the withheld observations to evaluate
431 the performance. The evaluation process was repeated for each of the 60 cities and the
432 performance was compared to that with individual inventories (shown in Table S3). The results
433 show that the ensemble predictions are better than those with EDGAR, MEIC, REAS2 and SOE
434 at 36, 37, 32 and 40 cities for $\text{PM}_{2.5}$, and 39, 39, 43, and 38 cities for O_3 -1h, respectively. The
435 ensemble predictions are better than ≥ 2 of the individual predictions at 45 and 41 cities for
436 $\text{PM}_{2.5}$ and O_3 -1h, respectively. Out of the 15 cities that the ensemble $\text{PM}_{2.5}$ is only better than
437 one or none of the individual predictions, 10 cities have MFB within ± 0.25 and MFE less than
438 0.25. Out of the 19 cities that the ensemble O_3 -1h is only better than one or none of the
439 individual predictions, 14 cities still have MNB within ± 0.2 and MNE less than 0.2. The results
440 demonstrate that the ensemble can improve the predictions even at locations with no
441 observational data available.
442

443 Previous studies have revealed that CTMs predictions agree more when averaging over longer
444 times (i.e., annual vs. monthly vs. daily averages) (Hu et al., 2014b; Hu et al., 2015b). Ensemble
445 predictions were also calculated with daily and monthly averages for $\text{PM}_{2.5}$, in addition to the
446 calculation with annual averages discussed above. The weighting factors and the performance of
447 ensemble predictions are shown in Table 2 and Figure 7, respectively. The weighting factors
448 vary largely with the averaging times, suggesting that the prediction optimization need to be

449 conducted separately when using different time averages. The ensemble predictions improve the
450 agreement with observations in all averaging time cases, with lower MNB and MNE than any of
451 the individual predictions. In general, EDGAR and REAS have large weights for daily and
452 monthly ensemble calculations, and MEIC and SOE have large weights for annual ensemble
453 calculations. This result indicates that the annual total emission rates of MEIC and SOE are
454 likely accurate but the temporal profiles to allocate the annual total emissions rates to specific
455 day/hours need to be improved.

456
457 Table 3 shows the ensemble prediction performance on PM_{2.5} and O₃-1h in different regions of
458 China using the daily average observations and daily average predictions with individual
459 inventories. The weighting factors vary greatly among regions, reflecting that substantial
460 difference in the spatial distributions of PM_{2.5} and O₃ when using different inventories. The
461 MNB and MNE values of ensemble predictions are reduced in all regions for both pollutants,
462 suggesting the ensemble predictions improve the accuracy and can be better used in further
463 health effects studies. The similar findings are also found with the monthly average observations
464 and predictions (shown in Table S4).

465
466 Figure 8 shows spatial distributions of PM_{2.5} and its components from the ensemble predictions
467 using the weighting factors of annual averages. The ensemble of PM_{2.5} components were
468 calculated using the same weighting factors for PM_{2.5}. Over 80 μg m⁻³ annual average PM_{2.5}
469 concentrations are estimated in NCP, CNT, YRD and SCB regions in 2013. Secondary inorganic
470 aerosols (SO₄²⁻, NO₃⁻, and NH₄⁺) account for approximately half of PM_{2.5}, and exhibit similar
471 spatial patterns. Carbonaceous aerosols (EC, POA, and SOA) account for about 30%, but POA
472 and SOA have quite different spatial distributions. High POA concentrations are mainly
473 distributed in NCP, CNT and SCB, while high SOA concentrations are found in the south part of
474 China. By considering the spatial distributions of population and ensemble PM_{2.5}, the population-
475 weighted annual averaged PM_{2.5} concentration in China in 2013 is 59.5 μg m⁻³, which is higher
476 than the estimated value of 54.8 μg m⁻³ by Brauer et al. (2016).

477
478 The products of the current study can be further applied in health effects studies. The first such
479 analysis used the annual PM_{2.5} ensemble predictions to assess the spatial distribution of excess
480 mortality due to adult (> 30 years old) ischemic heart disease (IHD), cerebrovascular disease
481 (CEV), chronic obstructive pulmonary disease (COPD) and lung cancer (LC) in China caused by
482 PM_{2.5} exposure (Hu et al., 2017a). Any health studies requiring human exposure information to
483 different pollutants would benefit from this study. Even though the weighted factors vary
484 depending on the regions, averaging times and different study years, the ensemble method
485 proposed in this study is to minimize the difference between predictions and observations and
486 can be applied in different studies. The way to calculate the weighting factors depends on the
487 objectives of specific studies. But in general, more observation data used in the calculation, more
488 accurate the ensemble prediction would be.

489 490 **4. Conclusion**

491
492 In this study, air quality predictions in China in 2013 were conducted using the WRF/CMAQ
493 modeling system with anthropogenic emissions from four inventories including MEIC, SOE,
494 EDGAR, and REAS2. Model performance with the four inventories was evaluated by comparing

495 with available observation data from 422 sites in 60 cities in China. Model predictions of hourly
496 O₃ and PM_{2.5} with the four inventories generally meet the model performance criteria, but that
497 model performance with different inventories varies on different pollutants and in different
498 regions. To improve the overall agreement of the predicted concentrations with observations,
499 ensemble predictions were calculated by linearly combining the predictions from different
500 inventories. The ensemble annual concentrations show improved agreement with observations
501 for both PM_{2.5} and O₃-1h. The MFB and MFE of the ensemble predictions of PM_{2.5} at the 60
502 cities are -0.11 and 0.24, respectively, which are better than the MFB (-0.25 – -0.16) and MFE
503 (0.26 – 0.31) of any individual simulations. The ensemble predictions of annual O₃-1h have the
504 MNB and MNE of 0.03 and 0.14, improved from MNB (0.06 – 0.19) and MNE (0.16 – 0.22) in
505 individual predictions. The ensemble predictions with data withholding method at each city show
506 better performance than the predictions with individual inventories at most cities, demonstrating
507 the ability of the ensemble in improving the predictions at locations where observational data are
508 not available. The ensemble predictions agree better with observations with daily, monthly, and
509 annual averaging times in all regions of China. The study demonstrates that ensemble predictions
510 by combining predictions from individual emission inventories can improve the accuracy in the
511 concentration estimation and the spatial distributions of air pollutants. The data presented in the
512 paper is available for downloading via requests.
513

514 **Acknowledgement**

515
516 This project is partly supported by the National Natural Science Foundation of China under
517 contract No. 41675125, Natural Science Foundation of Jiangsu Province under contract No.
518 BK20150904, Jiangsu Distinguished Professor Project 2191071503201, Jiangsu Six Major
519 Talent Peak Project 2015-JNHB-010, and the Priority Academic Program Development of
520 Jiangsu Higher Education Institutions (PAPD), Jiangsu Key Laboratory of Atmospheric
521 Environment Monitoring and Pollution Control of Nanjing University of Information Science
522 and Technology, and Jiangsu Province Innovation Platform for Superiority Subject of
523 Environmental Science and Engineering (No. KHK1201). The authors want to acknowledge the
524 Texas A&M Supercomputing Facility (<http://sc.tamu.edu>) and the Texas Advanced Computing
525 Center (<http://www.tacc.utexas.edu/>) for providing computing resources essential for completing
526 the research reported in this paper.

527 **References**

- 528
- 529 Akimoto, H., Ohara, T., Kurokawa, J.-i., and Horii, N.: Verification of energy consumption in
530 China during 1996–2003 by using satellite observational data, *Atmospheric Environment*, 40,
531 7663-7667, <http://dx.doi.org/10.1016/j.atmosenv.2006.07.052>, 2006.
- 532 Bin, Z., Shuxiao, W., Xinyi, D., Jiandong, W., Lei, D., Xiao, F., Jiming, H., and Joshua, F.:
533 Environmental effects of the recent emission changes in China: implications for particulate
534 matter pollution and soil acidification, *Environmental Research Letters*, 8, 024031, 2013.
- 535 Boylan, J. W., and Russell, A. G.: PM and light extinction model performance metrics, goals,
536 and criteria for three-dimensional air quality models, *Atmospheric Environment*, 40, 4946-4959,
537 2006.
- 538 Brauer, M., Freedman, G., Frostad, J., van Donkelaar, A., Martin, R. V., Dentener, F., Dingenen,
539 R. v., Estep, K., Amini, H., Apte, J. S., Balakrishnan, K., Barregard, L., Broday, D., Feigin, V.,
540 Ghosh, S., Hopke, P. K., Knibbs, L. D., Kokubo, Y., Liu, Y., Ma, S., Morawska, L., Sangrador, J.
541 L. T., Shaddick, G., Anderson, H. R., Vos, T., Forouzanfar, M. H., Burnett, R. T., and Cohen, A.:
542 Ambient Air Pollution Exposure Estimation for the Global Burden of Disease 2013, *Environ Sci*
543 *Technol*, 50, 79-88, 10.1021/acs.est.5b03709, 2016.
- 544 Byun, D., and Schere, K. L.: Review of the Governing Equations, Computational Algorithms,
545 and Other Components of the Models-3 Community Multiscale Air Quality (CMAQ) Modeling
546 System, *Applied Mechanics Reviews*, 59, 51-77, 2006.
- 547 Carter, W. P. L., and Heo, G.: Development of revised SAPRC aromatics mechanisms. Final
548 Report to the California Air Resources Board, Contracts No. 07-730 and 08-326, April 12, 2012. ,
549 2012.
- 550 Delle Monache, L., Deng, X. X., Zhou, Y. M., and Stull, R.: Ozone ensemble forecasts: 1. A new
551 ensemble design, *J Geophys Res-Atmos*, 111, 18, 10.1029/2005jd006310, 2006.
- 552 EPA, U. S.: Guidance for Demonstrating Attainment of Air Quality Goals for PM_{2.5} and
553 Regional Haze. Draft 2.1, 2 January 2001, in, edited by: The US Environmental Protection
554 Agency, O. o. A. a. R. O. o. A. P. a. S., Research Triangle, NC, 2001a.
- 555 EPA, U. S.: Guidance for Demonstrating Attainment of Air Quality Goals for PM_{2.5} and
556 Regional Haze. Draft 2.1, 2 January 2001, in, edited by: The US Environmental Protection
557 Agency, O. o. A. a. R. O. o. A. P. a. S., Research Triangle, NC, 2001b.
- 558 Guenther, A. B., Jiang, X., Heald, C. L., Sakulyanontvittaya, T., Duhl, T., Emmons, L. K., and
559 Wang, X.: The Model of Emissions of Gases and Aerosols from Nature version 2.1
560 (MEGAN2.1): an extended and updated framework for modeling biogenic emissions, *Geosci*
561 *Model Dev*, 5, 1471-1492, 10.5194/gmd-5-1471-2012, 2012.
- 562 Hu, J., Ying, Q., Chen, J. J., Mahmud, A., Zhao, Z., Chen, S. H., and Kleeman, M. J.: Particulate
563 air quality model predictions using prognostic vs. diagnostic meteorology in central California,
564 *Atmos Environ*, 44, 215-226, 10.1016/j.atmosenv.2009.10.011, 2010.
- 565 Hu, J., Wang, Y., Ying, Q., and Zhang, H.: Spatial and temporal variability of PM_{2.5} and PM₁₀
566 over the North China Plain and the Yangtze River Delta, China, *Atmospheric Environment*, 95,
567 598-609, <http://dx.doi.org/10.1016/j.atmosenv.2014.07.019>, 2014a.
- 568 Hu, J., Zhang, H., Chen, S.-H., Vandenberghe, F., Ying, Q., and Kleeman, M. J.: Predicting
569 Primary PM_{2.5} and PM_{0.1} Trace Composition for Epidemiological Studies in California,
570 *Environ Sci Technol*, 48, 4971-4979, 10.1021/es404809j, 2014b.
- 571 Hu, J., Zhang, H., Chen, S., Ying, Q., Vandenberghe, F., and Kleeman, M. J.: Identifying PM_{2.5}
572 and PM_{0.1} Sources for Epidemiological Studies in California, *Environ Sci Technol*, 48, 4980-
573 4990, 10.1021/es404810z, 2014c.

574 Hu, J., Wu, L., Zheng, B., Zhang, Q., He, K., Chang, Q., Li, X., Yang, F., Ying, Q., and Zhang,
575 H.: Source contributions and regional transport of primary particulate matter in China,
576 *Environmental Pollution*, 207, 31-42, 2015a.

577 Hu, J., Zhang, H., Ying, Q., Chen, S.-H., Vandenberghe, F., and Kleeman, M. J.: Long-term
578 particulate matter modeling for health effect studies in California - Part I: model performance on
579 temporal and spatial variations, *Atmos Chem Phys*, 15, 3445-3461, 2015b.

580 Hu, J., Chen, J., Ying, Q., and Zhang, H.: One-year Simulation of Ozone and Particulate Matter
581 in China Using WRF/CMAQ Modeling System, *Atmos. Chem. Phys.*, 16, 10333-10350, 2016a.

582 Hu, J., Jathar, S., Zhang, H., Ying, Q., Chen, S. H., Cappa, C. D., and Kleeman, M. J.: Long-
583 term Particulate Matter Modeling for Health Effects Studies in California – Part II:
584 Concentrations and Sources of Ultrafine Organic Aerosols, *Atmos. Chem. Phys. Discuss.*, 2016,
585 1-37, 10.5194/acp-2016-903, 2016b.

586 Hu, J., Huang, L., Chen, M., Liao, H., Zhang, H., Wang, S., Zhang, Q., and Ying, Q.: Premature
587 Mortality Attributable to Particulate Matter in China: Source Contributions and Responses to
588 Reductions, *Environ Sci Technol*, 10.1021/acs.est.7b03193, 2017a.

589 Hu, J., Wang, P., Ying, Q., Zhang, H., Chen, J., Ge, X., Li, X., Jiang, J., Wang, S., Zhang, J.,
590 Zhao, Y., and Zhang, Y.: Modeling biogenic and anthropogenic secondary organic aerosol in
591 China, *Atmos. Chem. Phys.*, 17, 77-92, 10.5194/acp-17-77-2017, 2017b.

592 Hu, Y. T., Odman, M. T., and Russell, A. G.: Mass conservation in the Community Multiscale
593 Air Quality model, *Atmos Environ*, 40, 1199-1204, DOI 10.1016/j.atmosenv.2005.10.038, 2006.

594 Huang, C., Chen, C. H., Li, L., Cheng, Z., Wang, H. L., Huang, H. Y., Streets, D. G., Wang, Y.
595 J., Zhang, G. F., and Chen, Y. R.: Emission inventory of anthropogenic air pollutants and VOC
596 species in the Yangtze River Delta region, China, *Atmos. Chem. Phys.*, 11, 4105-4120,
597 10.5194/acp-11-4105-2011, 2011.

598 Huijnen, V., Eskes, H. J., Poupkou, A., Elbern, H., Boersma, K. F., Foret, G., Sofiev, M.,
599 Valdebenito, A., Flemming, J., Stein, O., Gross, A., Robertson, L., D'Isidoro, M., Kioutsioukis, I.,
600 Friese, E., Amstrup, B., Bergstrom, R., Strunk, A., Vira, J., Zyryanov, D., Maurizi, A., Melas, D.,
601 Peuch, V. H., and Zerefos, C.: Comparison of OMI NO₂ tropospheric columns with an ensemble
602 of global and European regional air quality models, *Atmos Chem Phys*, 10, 3273-3296, 2010.

603 Kurokawa, J., Ohara, T., Morikawa, T., Hanayama, S., Janssens-Maenhout, G., Fukui, T.,
604 Kawashima, K., and Akimoto, H.: Emissions of air pollutants and greenhouse gases over Asian
605 regions during 2000–2008: Regional Emission inventory in ASia (REAS) version 2, *Atmos.*
606 *Chem. Phys.*, 13, 11019-11058, 10.5194/acp-13-11019-2013, 2013.

607 Laurent, O., Hu, J., Li, L., Kleeman, M. J., Bartell, S. M., Cockburn, M., Escobedo, L., and Wu,
608 J.: A Statewide Nested Case-Control Study of Preterm Birth and Air Pollution by Source and
609 Composition: California, 2001-2008, *Environ Health Persp*,
610 <http://dx.doi.org/10.1289/ehp.1510133>, 2016a.

611 Laurent, O., Hu, J. L., Li, L. F., Kleeman, M. J., Bartell, S. M., Cockburn, M., Escobedo, L., and
612 Wu, J.: Low birth weight and air pollution in California: Which sources and components drive
613 the risk?, *Environ Int*, 92-93, 471-477, 10.1016/j.envint.2016.04.034, 2016b.

614 Lei, Y., Zhang, Q., He, K. B., and Streets, D. G.: Primary anthropogenic aerosol emission trends
615 for China, 1990–2005, *Atmos. Chem. Phys.*, 11, 931-954, 10.5194/acp-11-931-2011, 2011a.

616 Lei, Y., Zhang, Q., Nielsen, C., and He, K.: An inventory of primary air pollutants and CO₂
617 emissions from cement production in China, 1990–2020, *Atmospheric Environment*, 45, 147-154,
618 <http://dx.doi.org/10.1016/j.atmosenv.2010.09.034>, 2011b.

619 Lelieveld, J., Evans, J. S., Fnais, M., Giannadaki, D., and Pozzer, A.: The contribution of outdoor
620 air pollution sources to premature mortality on a global scale, *Nature*, 525, 367-+,
621 10.1038/nature15371, 2015a.

622 Lelieveld, J., Evans, J. S., Fnais, M., Giannadaki, D., and Pozzer, A.: The contribution of outdoor
623 air pollution sources to premature mortality on a global scale, *Nature*, 525, 367-371,
624 10.1038/nature15371, 2015b.

625 Li, J., Cleveland, M., Ziemba, L. D., Griffin, R. J., Barsanti, K. C., Pankow, J. F., and Ying, Q.:
626 Modeling regional secondary organic aerosol using the Master Chemical Mechanism, *Atmos*
627 *Environ*, 102, 52-61, <http://dx.doi.org/10.1016/j.atmosenv.2014.11.054>, 2015.

628 Li, M., Zhang, Q., Streets, D. G., He, K. B., Cheng, Y. F., Emmons, L. K., Huo, H., Kang, S. C.,
629 Lu, Z., Shao, M., Su, H., Yu, X., and Zhang, Y.: Mapping Asian anthropogenic emissions of
630 non-methane volatile organic compounds to multiple chemical mechanisms, *Atmos. Chem. Phys.*,
631 14, 5617-5638, 10.5194/acp-14-5617-2014, 2014.

632 Liu, J., Han, Y., Tang, X., Zhu, J., and Zhu, T.: Estimating adult mortality attributable to PM2.5
633 exposure in China with assimilated PM2.5 concentrations based on a ground monitoring network,
634 *Sci Total Environ*, <http://dx.doi.org/10.1016/j.scitotenv.2016.05.165>, 2016.

635 Murphy, J. M., Sexton, D. M. H., Barnett, D. N., Jones, G. S., Webb, M. J., Collins, M., and
636 Stainforth, D. A.: Quantification of modelling uncertainties in a large ensemble of climate
637 change simulations, *Nature*, 430, 768-772, 10.1038/nature02771, 2004.

638 Ostro, B., Hu, J., Goldberg, D., Reynolds, P., Hertz, A., Bernstein, L., and Kleeman, M. J.:
639 Associations of Mortality with Long-Term Exposures to Fine and Ultrafine Particles, *Species*
640 *and Sources: Results from the California Teachers Study Cohort*, *Environ Health Persp*,
641 DOI:10.1289/ehp.1408565, 2015.

642 Ou, J., Zheng, J., Li, R., Huang, X., Zhong, Z., Zhong, L., and Lin, H.: Speciated OVOC and
643 VOC emission inventories and their implications for reactivity-based ozone control strategy in
644 the Pearl River Delta region, China, *Sci Total Environ*, 530-531, 393-402,
645 <http://dx.doi.org/10.1016/j.scitotenv.2015.05.062>, 2015.

646 Philip, S., Martin, R. V., van Donkelaar, A., Lo, J. W.-H., Wang, Y., Chen, D., Zhang, L.,
647 Kasibhatla, P. S., Wang, S., Zhang, Q., Lu, Z., Streets, D. G., Bittman, S., and Macdonald, D. J.:
648 Global Chemical Composition of Ambient Fine Particulate Matter for Exposure Assessment,
649 *Environ Sci Technol*, 48, 13060-13068, 10.1021/es502965b, 2014.

650 Qiao, X., Tang, Y., Hu, J., Zhang, S., Li, J., Kota, S. H., Wu, L., Gao, H., Zhang, H., and Ying,
651 Q.: Modeling dry and wet deposition of sulfate, nitrate, and ammonium ions in Jiuzhaigou
652 National Nature Reserve, China using a source-oriented CMAQ model: Part I. Base case model
653 results, *Sci Total Environ*, 532, 831-839, <http://dx.doi.org/10.1016/j.scitotenv.2015.05.108>, 2015.

654 Saikawa, E., Kim, H., Zhong, M., Zhao, Y., Janssens-Manehout, G., Kurokawa, J. I., Klimont, Z.,
655 Wagner, F., Naik, V., Horowitz, L., and Zhang, Q.: Comparison of Emissions Inventories of
656 Anthropogenic Air Pollutants in China, *Atmos. Chem. Phys. Discuss.*, 2016, 1-41, 10.5194/acp-
657 2016-888, 2016.

658 Skamarock, W. C., Klemp, J. B., Dudhia, J., Gill, D. O., Barker, D. M., Duda, M. G., Huang, X.-
659 Y., Wang, W., and Powers, J. G.: A Description of the Advanced Research WRF Version 3,
660 NCAR Technical Note NCAR/TN-475+STR, 2008.

661 Streets, D. G., Bond, T. C., Carmichael, G. R., Fernandes, S. D., Fu, Q., He, D., Klimont, Z.,
662 Nelson, S. M., Tsai, N. Y., Wang, M. Q., Woo, J. H., and Yarber, K. F.: An inventory of gaseous
663 and primary aerosol emissions in Asia in the year 2000, *Journal of Geophysical Research-*
664 *Atmospheres*, 108, 8809

665 10.1029/2002jd003093, 2003.

666 Su, S., Li, B., Cui, S., and Tao, S.: Sulfur Dioxide Emissions from Combustion in China: From
667 1990 to 2007, *Environmental Science & Technology*, 45, 8403-8410, 10.1021/es201656f, 2011.

668 Tao, J., Gao, J., Zhang, L., Zhang, R., Che, H., Zhang, Z., Lin, Z., Jing, J., Cao, J., and Hsu, S.
669 C.: PM_{2.5} pollution in a megacity of southwest China: source apportionment and implication,
670 *Atmos. Chem. Phys.*, 14, 8679-8699, 10.5194/acp-14-8679-2014, 2014.

671 Tebaldi, C., and Knutti, R.: The use of the multi-model ensemble in probabilistic climate
672 projections, *Philos. Trans. R. Soc. A-Math. Phys. Eng. Sci.*, 365, 2053-2075,
673 10.1098/rsta.2007.2076, 2007.

674 Wang, D., Hu, J., Xu, Y., Lv, D., Xie, X., Kleeman, M., Xing, J., Zhang, H., and Ying, Q.:
675 Source contributions to primary and secondary inorganic particulate matter during a severe
676 wintertime PM_{2.5} pollution episode in Xi'an, China, *Atmospheric Environment*, 97, 182-194,
677 <http://dx.doi.org/10.1016/j.atmosenv.2014.08.020>, 2014a.

678 Wang, S., Xing, J., Chatani, S., Hao, J., Klimont, Z., Cofala, J., and Amann, M.: Verification of
679 anthropogenic emissions of China by satellite and ground observations, *Atmos Environ*, 45,
680 6347-6358, <http://dx.doi.org/10.1016/j.atmosenv.2011.08.054>, 2011.

681 Wang, S. W., Zhang, Q., Streets, D. G., He, K. B., Martin, R. V., Lamsal, L. N., Chen, D., Lei,
682 Y., and Lu, Z.: Growth in NO_x emissions from power plants in China: bottom-up estimates and
683 satellite observations, *Atmos. Chem. Phys.*, 12, 4429-4447, 10.5194/acp-12-4429-2012, 2012.

684 Wang, X., Liang, X.-Z., Jiang, W., Tao, Z., Wang, J. X. L., Liu, H., Han, Z., Liu, S., Zhang, Y.,
685 Grell, G. A., and Peckham, S. E.: WRF-Chem simulation of East Asian air quality: Sensitivity to
686 temporal and vertical emissions distributions, *Atmos Environ*, 44, 660-669, 2010.

687 Wang, Y., Ying, Q., Hu, J., and Zhang, H.: Spatial and temporal variations of six criteria air
688 pollutants in 31 provincial capital cities in China during 2013–2014, *Environment International*,
689 73, 413-422, <http://dx.doi.org/10.1016/j.envint.2014.08.016>, 2014b.

690 Wiedinmyer, C., Akagi, S. K., Yokelson, R. J., Emmons, L. K., Al-Saadi, J. A., Orlando, J. J.,
691 and Soja, A. J.: The Fire INventory from NCAR (FINN): a high resolution global model to
692 estimate the emissions from open burning, *Geoscientific Model Development*, 4, 625-641, 2011.

693 Xu, Y., Hu, J., Ying, Q., Wang, D., and Zhang, H.: Current and future emissions of primary
694 pollutants from coal-fired power plants in Shaanxi, China, *Science of the total environment*, In
695 revision, 2017.

696 Ying, Q., Cureño, I. V., Chen, G., Ali, S., Zhang, H., Malloy, M., Bravo, H. A., and Sosa, R.:
697 Impacts of Stabilized Criegee Intermediates, surface uptake processes and higher aromatic
698 secondary organic aerosol yields on predicted PM_{2.5} concentrations in the Mexico City
699 Metropolitan Zone, *Atmos Environ*, 94, 438-447,
700 <http://dx.doi.org/10.1016/j.atmosenv.2014.05.056>, 2014.

701 Ying, Q., Li, J., and Kota, S. H.: Significant Contributions of Isoprene to Summertime
702 Secondary Organic Aerosol in Eastern United States, *Environ Sci Technol*, 49, 7834-7842,
703 10.1021/acs.est.5b02514, 2015.

704 Yu, S. C., Dennis, R., Roselle, S., Nenes, A., Walker, J., Eder, B., Schere, K., Swall, J., and
705 Robarge, W.: An assessment of the ability of three-dimensional air quality models with current
706 thermodynamic equilibrium models to predict aerosol NO₃-, *J Geophys Res-Atmos*, 110, 2005.

707 Zhang, H., Li, J., Ying, Q., Yu, J. Z., Wu, D., Cheng, Y., He, K., and Jiang, J.: Source
708 apportionment of PM_{2.5} nitrate and sulfate in China using a source-oriented chemical transport
709 model, *Atmospheric Environment*, 62, 228-242, 10.1016/j.atmosenv.2012.08.014, 2012.

710 Zhang, Q., Wei, Y., Tian, W., and Yang, K.: GIS-based emission inventories of urban scale: A
711 case study of Hangzhou, China, *Atmos Environ*, 42, 5150-5165,
712 <http://dx.doi.org/10.1016/j.atmosenv.2008.02.012>, 2008.

713 Zhang, Q., Streets, D. G., Carmichael, G. R., He, K. B., Huo, H., Kannari, A., Klimont, Z., Park,
714 I. S., Reddy, S., Fu, J. S., Chen, D., Duan, L., Lei, Y., Wang, L. T., and Yao, Z. L.: Asian
715 emissions in 2006 for the NASA INTEX-B mission, *Atmos Chem Phys*, 9, 5131-5153, 2009.

716 Zhang, X., Cappa, C. D., Jathar, S. H., McVay, R. C., Ensberg, J. J., Kleeman, M. J., and
717 Seinfeld, J. H.: Influence of vapor wall loss in laboratory chambers on yields of secondary
718 organic aerosol, *Proceedings of the National Academy of Sciences*, 111, 5802-5807,
719 10.1073/pnas.1404727111, 2014.

720 Zhang, Y.-L., and Cao, F.: Fine particulate matter (PM_{2.5}) in China at a city level, *Scientific*
721 *Reports*, 5, 14884, 10.1038/srep14884
722 <http://www.nature.com/articles/srep14884#supplementary-information>, 2015.

723 Zhao, B., Wang, P., Ma, J. Z., Zhu, S., Pozzer, A., and Li, W.: A high-resolution emission
724 inventory of primary pollutants for the Huabei region, China, *Atmos. Chem. Phys.*, 12, 481-501,
725 10.5194/acp-12-481-2012, 2012.

726 Zhao, B., Wang, S., Wang, J., Fu, J. S., Liu, T., Xu, J., Fu, X., and Hao, J.: Impact of national
727 NO_x and SO₂ control policies on particulate matter pollution in China, *Atmospheric*
728 *Environment*, 77, 453-463, <http://dx.doi.org/10.1016/j.atmosenv.2013.05.012>, 2013.

729 Zhao, Y., Wang, S., Duan, L., Lei, Y., Cao, P., and Hao, J.: Primary air pollutant emissions of
730 coal-fired power plants in China: Current status and future prediction, *Atmospheric Environment*,
731 42, 8442-8452, <http://dx.doi.org/10.1016/j.atmosenv.2008.08.021>, 2008.

732 Zhao, Y., Nielsen, C. P., Lei, Y., McElroy, M. B., and Hao, J.: Quantifying the uncertainties of a
733 bottom-up emission inventory of anthropogenic atmospheric pollutants in China, *Atmospheric*
734 *Chemistry and Physics*, 11, 2295-2308, 10.5194/acp-11-2295-2011, 2011.

735 Zheng, B., Huo, H., Zhang, Q., Yao, Z. L., Wang, X. T., Yang, X. F., Liu, H., and He, K. B.:
736 High-resolution mapping of vehicle emissions in China in 2008, *Atmos. Chem. Phys.*, 14, 9787-
737 9805, 10.5194/acp-14-9787-2014, 2014.

738 Zheng, J., Zhang, L., Che, W., Zheng, Z., and Yin, S.: A highly resolved temporal and spatial air
739 pollutant emission inventory for the Pearl River Delta region, China and its uncertainty
740 assessment, *Atmospheric Environment*, 43, 5112-5122,
741 <http://dx.doi.org/10.1016/j.atmosenv.2009.04.060>, 2009.

742
743

Table 1. Overall model performance of gas and PM species in 2013 using different inventories. Obs is observation, MFB is mean fractional bias, MFE is mean fractional error, MNB is mean normalized bias, and MNE is mean normalized error. The indices were calculated with hourly observations and predictions.

		Prediction	MFB	MFE	MNB	MNE
	Mean Obs: 51.70 ppb					
O ₃	MEIC	49.83	-0.08	0.35	0.02	0.33
	SOE	44.51	-0.2	0.38	-0.09	0.32
	EDGAR	49.82	-0.04	0.28	0.03	0.28
	REAS2	51.17	-0.04	0.33	0.05	0.33
	Mean Obs: 0.96 ppm					
CO	MEIC	0.31	-0.92	0.96	-0.57	0.63
	SOE	/	/	/	/	/
	EDGAR	0.23	-1.12	1.16	-0.66	0.73
	REAS2	0.42	-0.72	0.82	-0.41	0.59
	Mean Obs: 21.45 ppb					
NO ₂	MEIC	10.12	-0.79	0.93	-0.41	0.66
	SOE	11.59	-0.65	0.81	-0.33	0.61
	EDGAR	6.82	-1.02	1.07	-0.6	0.67
	REAS2	9.3	-0.81	0.92	-0.46	0.63
	Mean Obs: 17.21 ppb					
SO ₂	MEIC	12.5	-0.51	0.87	0.01	0.87
	SOE	12.76	-0.44	0.83	0.06	0.86
	EDGAR	15.86	-0.16	0.73	0.31	0.88
	REAS2	15.15	-0.23	0.74	0.23	0.86
	Mean Obs: 70.01 $\mu\text{g m}^{-3}$					
PM _{2.5}	MEIC	56.39	-0.32	0.64	-0.02	0.63
	SOE	59.77	-0.24	0.61	0.09	0.67
	EDGAR	52.59	-0.3	0.59	-0.05	0.56
	REAS2	60.35	-0.21	0.59	0.08	0.63
	Mean Obs: 118.61 $\mu\text{g m}^{-3}$					
PM ₁₀	MEIC	62.7	-0.63	0.79	-0.32	0.61
	SOE	63.32	-0.6	0.76	-0.3	0.6
	EDGAR	55.76	-0.67	0.78	-0.38	0.58
	REAS2	71.41	-0.49	0.7	-0.21	0.59

Table 2. The weighting factors (w) of each inventory in the ensemble predictions of $PM_{2.5}$ when using daily, monthly, or annual averages in the objective function (E5).

	Daily	Monthly	Annual
MEIC	0.07	0.13	0.31
SOE	0.14	0.16	0.24
EDGAR	0.38	0.23	0.20
REAS2	0.49	0.63	0.36

Table 3. Performance of daily PM_{2.5} (MFB and MFE) and O₃-1h (MNB and MNE) in different regions of China based on individual inventories and the ensemble. The weighting factors (w) used to calculate the ensemble of each region are also included.

	Region (# of Cities)	MEIC			SOE			EDGAR			REAS2			ENSEMBLE	
		w	MFB	MFE	w	MFB	MFE	w	MFB	MFE	w	MFB	MFE	MFB	MFE
PM _{2.5}	NE (4)	0.16	-0.23	0.44	0.21	0.38	0.68	0.20	-0.30	0.43	0.43	-0.12	0.43	-0.08	0.42
	NCP (14)	0.00	-0.30	0.47	0.52	-0.34	0.46	0.14	-0.40	0.51	0.56	-0.20	0.41	-0.12	0.40
	NW (6)	0.00	-0.87	0.90	0.20	-0.80	0.84	0.59	-0.85	0.87	1.00	-0.81	0.83	-0.49	0.66
	YRD (20)	0.05	-0.29	0.45	0.00	-0.27	0.43	0.61	-0.23	0.40	0.35	-0.13	0.40	-0.18	0.38
	CNT (5)	0.09	-0.10	0.46	0.18	-0.05	0.41	0.50	-0.27	0.40	0.22	0.09	0.44	-0.14	0.37
	SCB (2)	0.00	0.10	0.48	0.64	0.23	0.48	0.00	-0.10	0.39	0.08	0.07	0.43	-0.15	0.40
	SOUTH (9)	0.10	-0.35	0.51	0.00	-0.18	0.41	0.59	-0.07	0.45	0.30	-0.25	0.44	-0.16	0.41
	CHINA (60)	0.07	-0.34	0.52	0.14	-0.26	0.50	0.38	-0.33	0.49	0.49	-0.22	0.46	-0.20	0.45
		w	MNB	MNE	w	MNB	MNE	w	MNB	MNE	w	MNB	MNE	MNB	MNE
O ₃ -1h	NE	0.09	0.44	0.50	0.00	0.16	0.34	0.45	0.41	0.47	0.27	0.42	0.48	0.14	0.31
	NCP	0.29	0.33	0.47	0.12	0.23	0.44	0.06	0.46	0.59	0.42	0.47	0.56	0.25	0.43
	NW	0.00	0.65	0.72	0.82	0.54	0.62	0.00	0.70	0.77	0.00	0.68	0.74	0.25	0.46
	YRD	0.00	0.20	0.41	0.53	0.14	0.38	0.00	0.25	0.45	0.45	0.27	0.44	0.17	0.39
	CNT	0.27	0.27	0.47	0.18	0.16	0.43	0.10	0.35	0.53	0.36	0.35	0.52	0.18	0.42
	SCB	0.44	0.59	0.68	0.14	0.42	0.58	0.28	0.59	0.70	0.00	0.60	0.72	0.33	0.53
	SOUTH	0.84	0.39	0.50	0.00	0.29	0.46	0.00	0.38	0.51	0.00	0.42	0.53	0.16	0.37
	CHINA	0.19	0.34	0.49	0.20	0.23	0.44	0.00	0.39	0.54	0.51	0.41	0.53	0.21	0.42

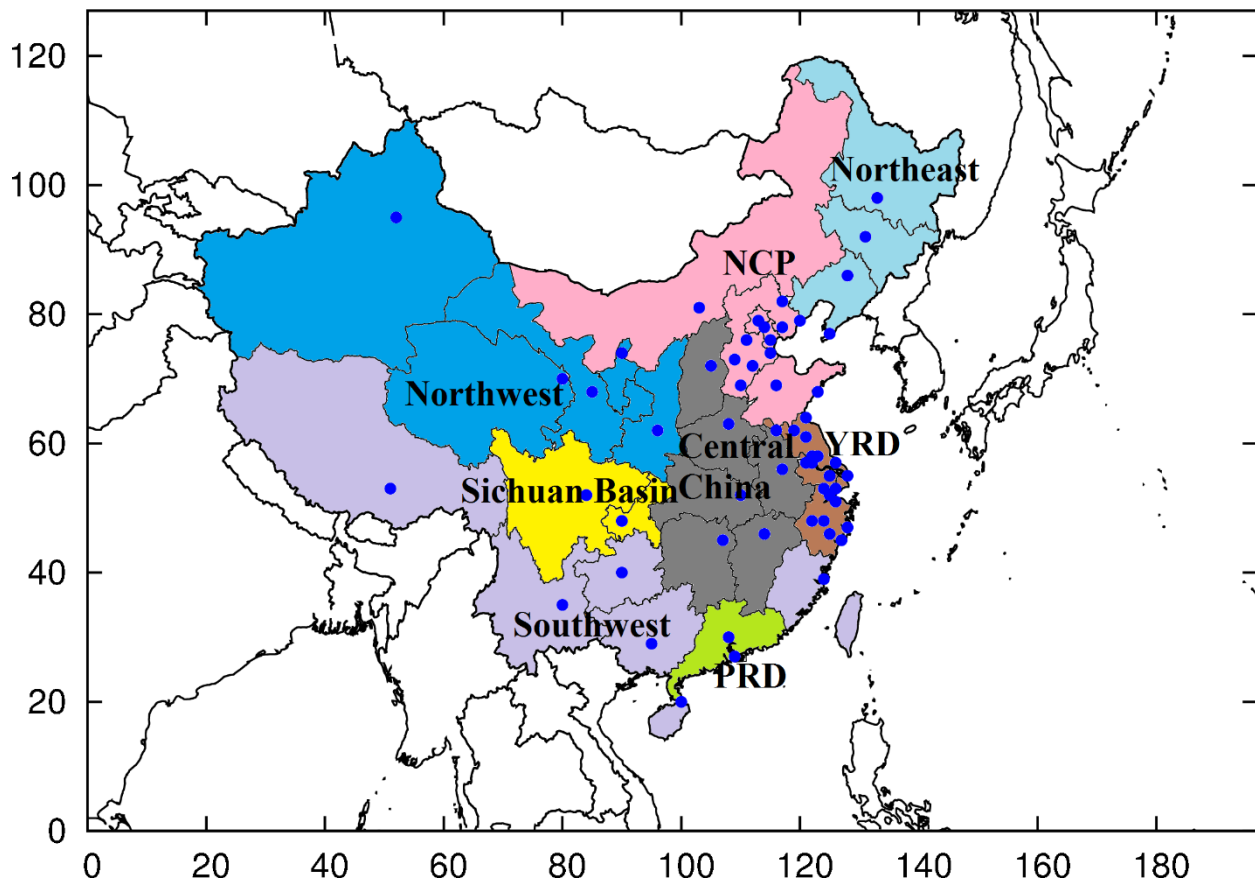


Figure 1. The WRF/CMAQ modeling domain and the regions in China. The dots represent the 60 cities where observational data are available for ensemble analysis.

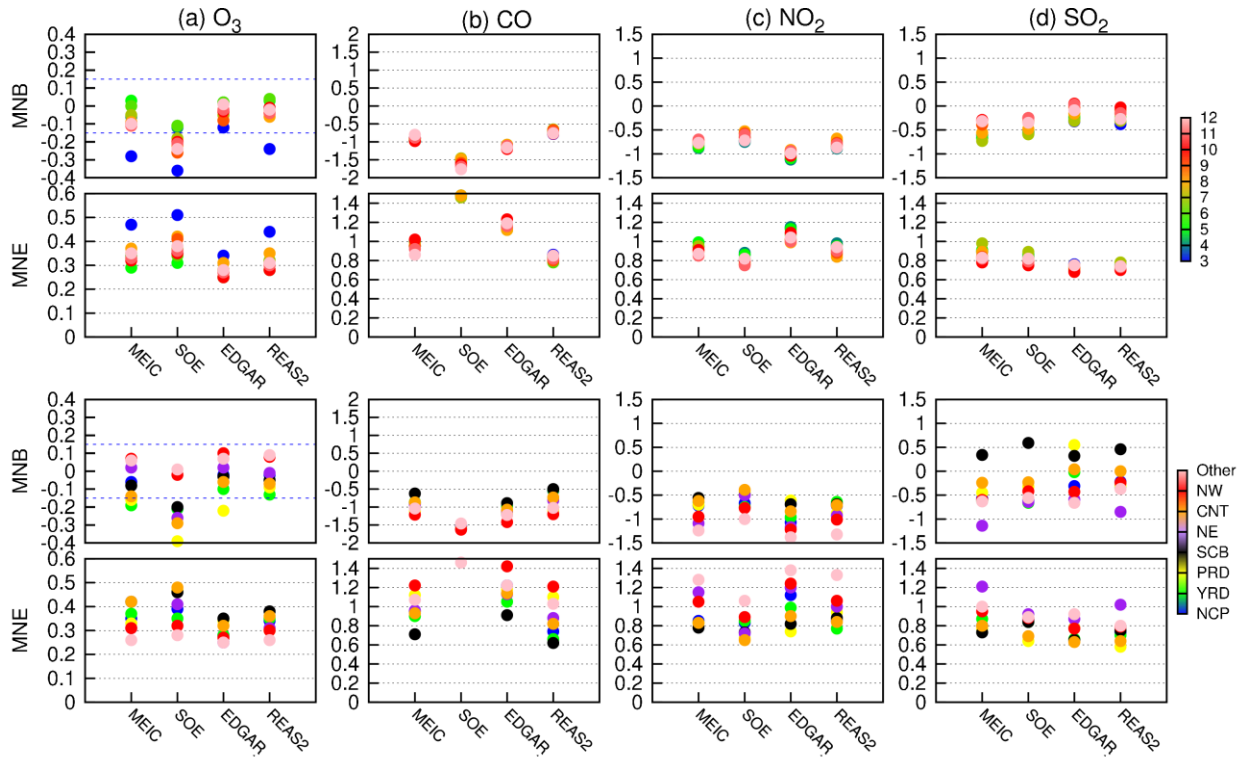


Figure 2. Performance of predicted O_3 , CO, NO_2 , and SO_2 for different months (top two rows) and regions based on simulations with individual inventories. The blue dashed lines on the O_3 plots are ± 0.15 for MNB and 0.3 for MNE as suggested by U. S. EPA (2001a). Changes of colors show the months from March to December in top two rows, while show regions from NCP to Other in the bottom two rows. The same for Figure 2.

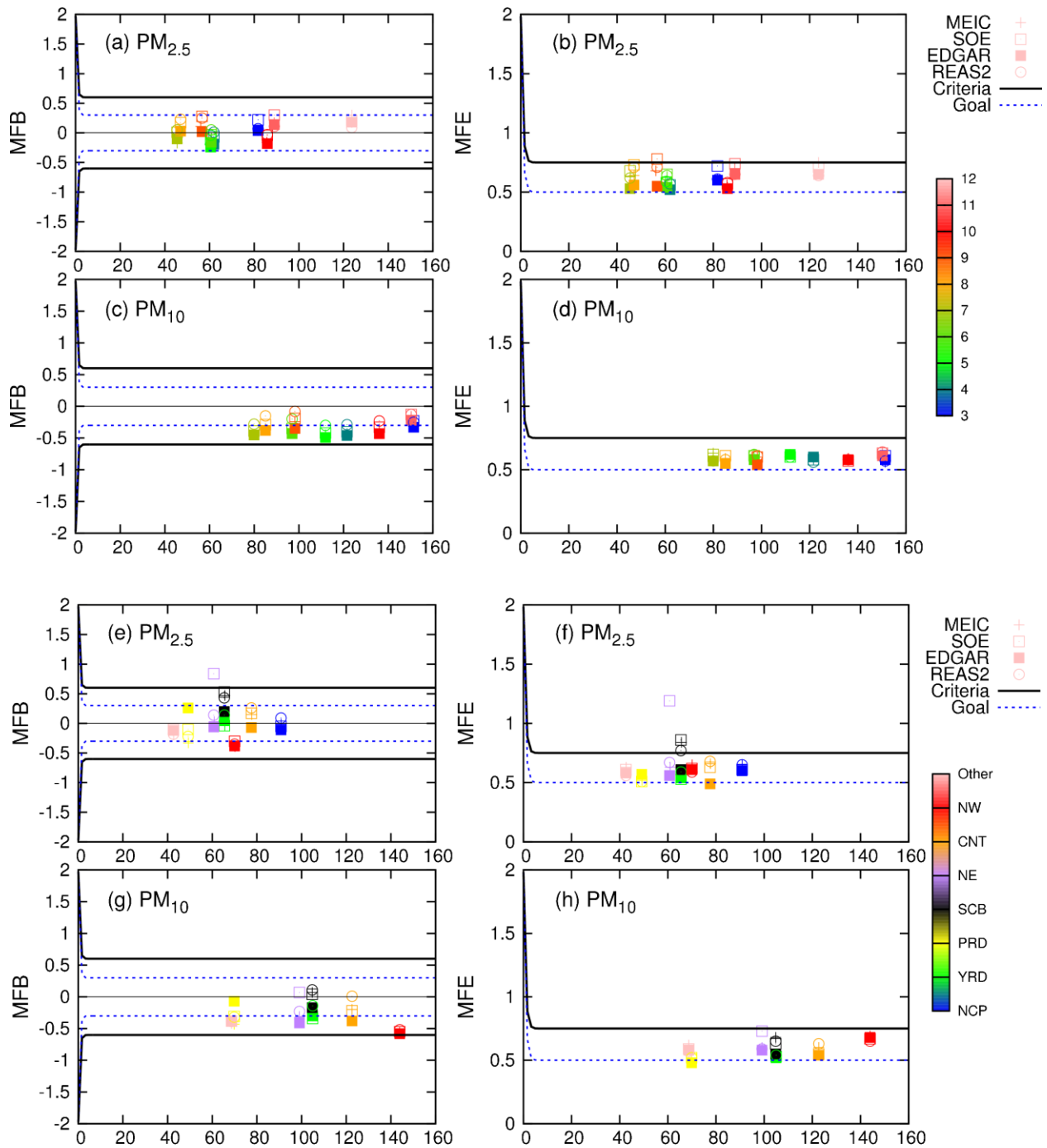


Figure 3. Performance of predicted $PM_{2.5}$ and PM_{10} for different months (a-d) and regions (e-h) based on simulations with individual inventories. The x-axis is the observed concentrations. The model performance criteria (solid black lines) and goals (dash blue lines) are suggested by Byun and Russell (2006). The model performance goals represent the level of accuracy that is considered to be close to the best a model can be expected to achieve, and the model performance criteria represent the level of accuracy that is considered to be acceptable for modeling applications.

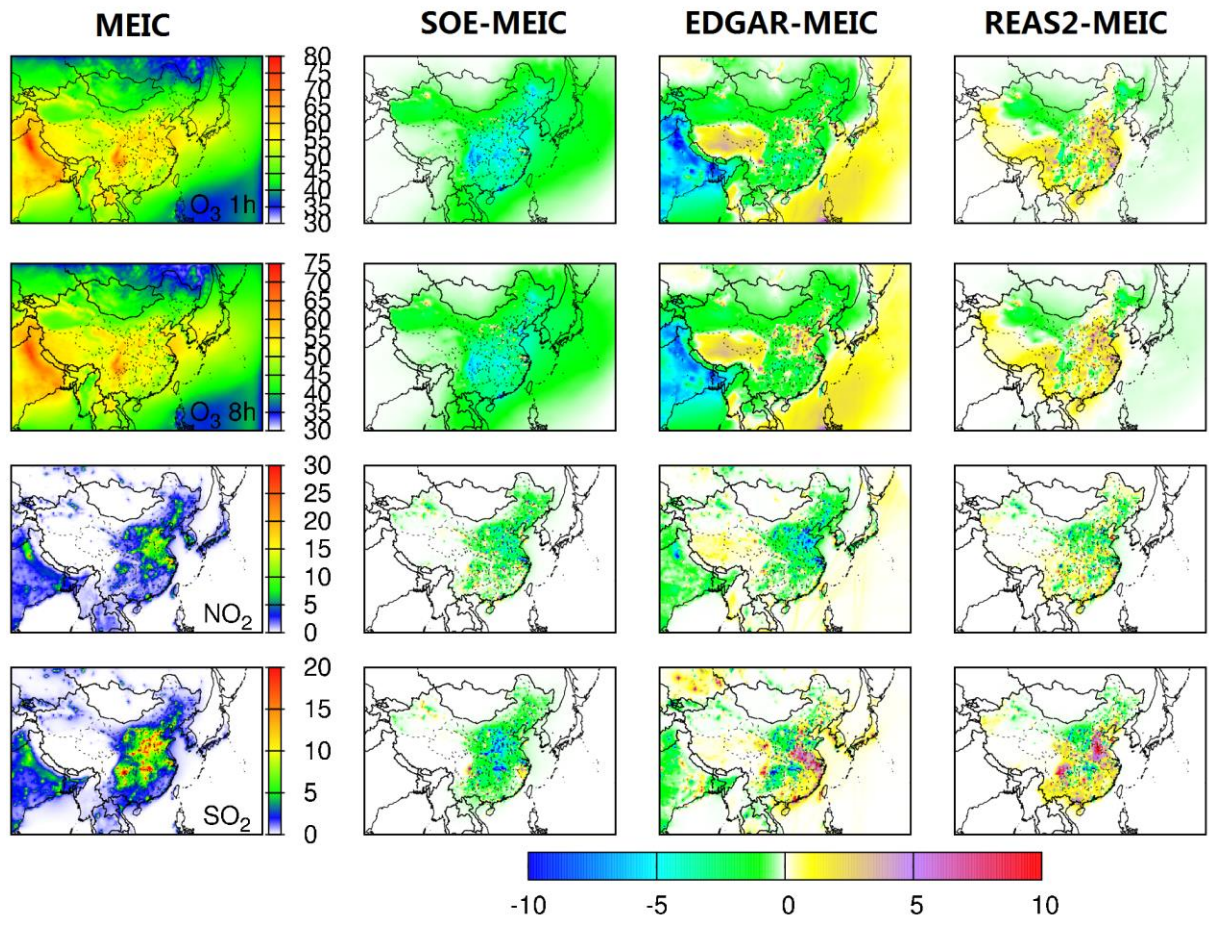


Figure 4. Spatial difference of model predicted annual averaged gas species concentrations (in the horizontal panels) with different inventories (in the vertical panels). Units are ppb. The color bars of the first column are different to better show the spatial distribution of different species. White indicates zero while blue, green, yellow and red means concentrations from low to high. The color bar for the other three columns are same, white indicates zero, blue and green mean values less than zero while yellow, purple and red mean values larger than zero. O₃-1h represents daily maximum 1h O₃ and O₃-8h represents daily maximum 8h mean O₃.

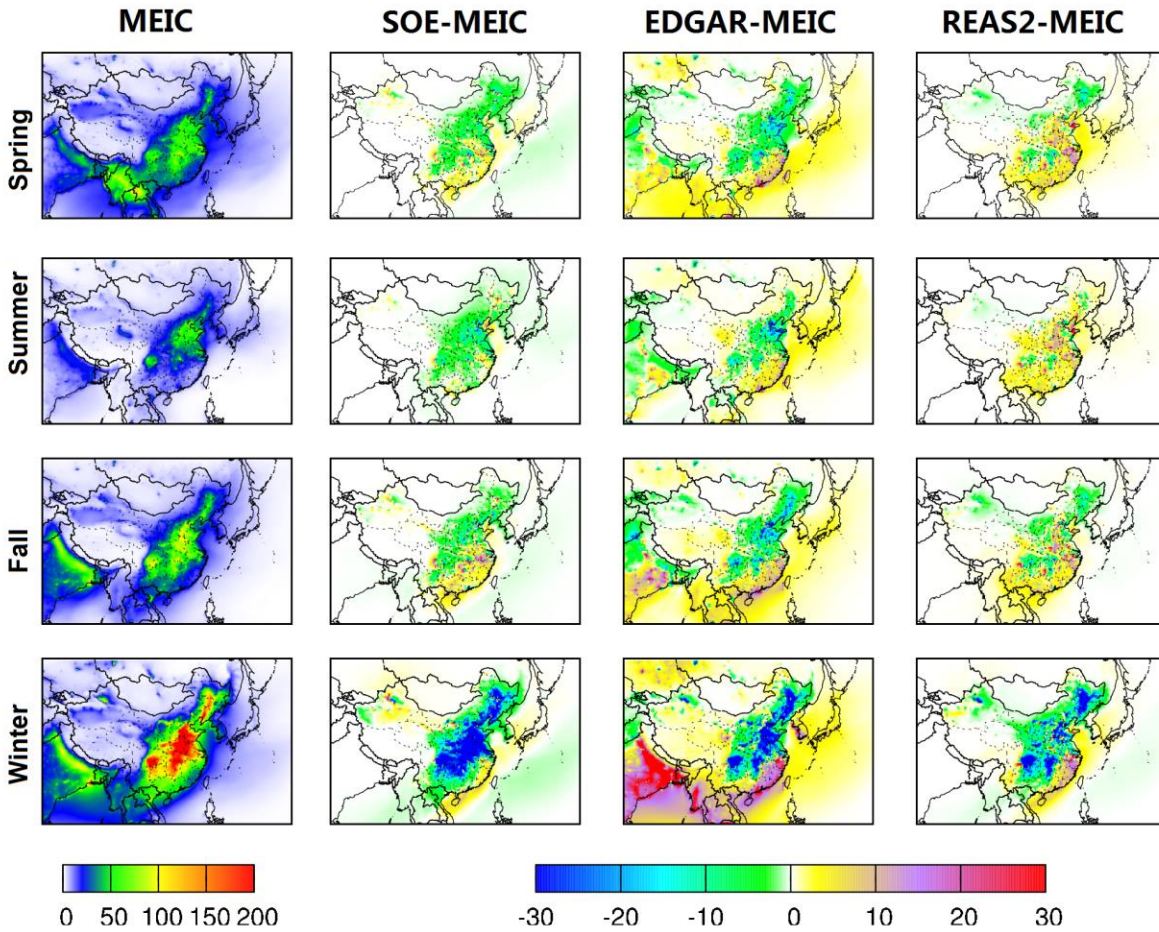


Figure 5. Spatial difference of model predicted seasonal averaged $PM_{2.5}$ concentrations (in the horizontal panels) with different inventories (in the vertical panels). Units are $\mu g m^{-3}$. In the first column, white indicates zero while blue, green, yellow and red means concentrations from low to high. The color bar for the other three columns are same, white indicates zero, blue and green mean values less than zero while yellow, purple and red mean values larger than zero. The same for Figure 6.

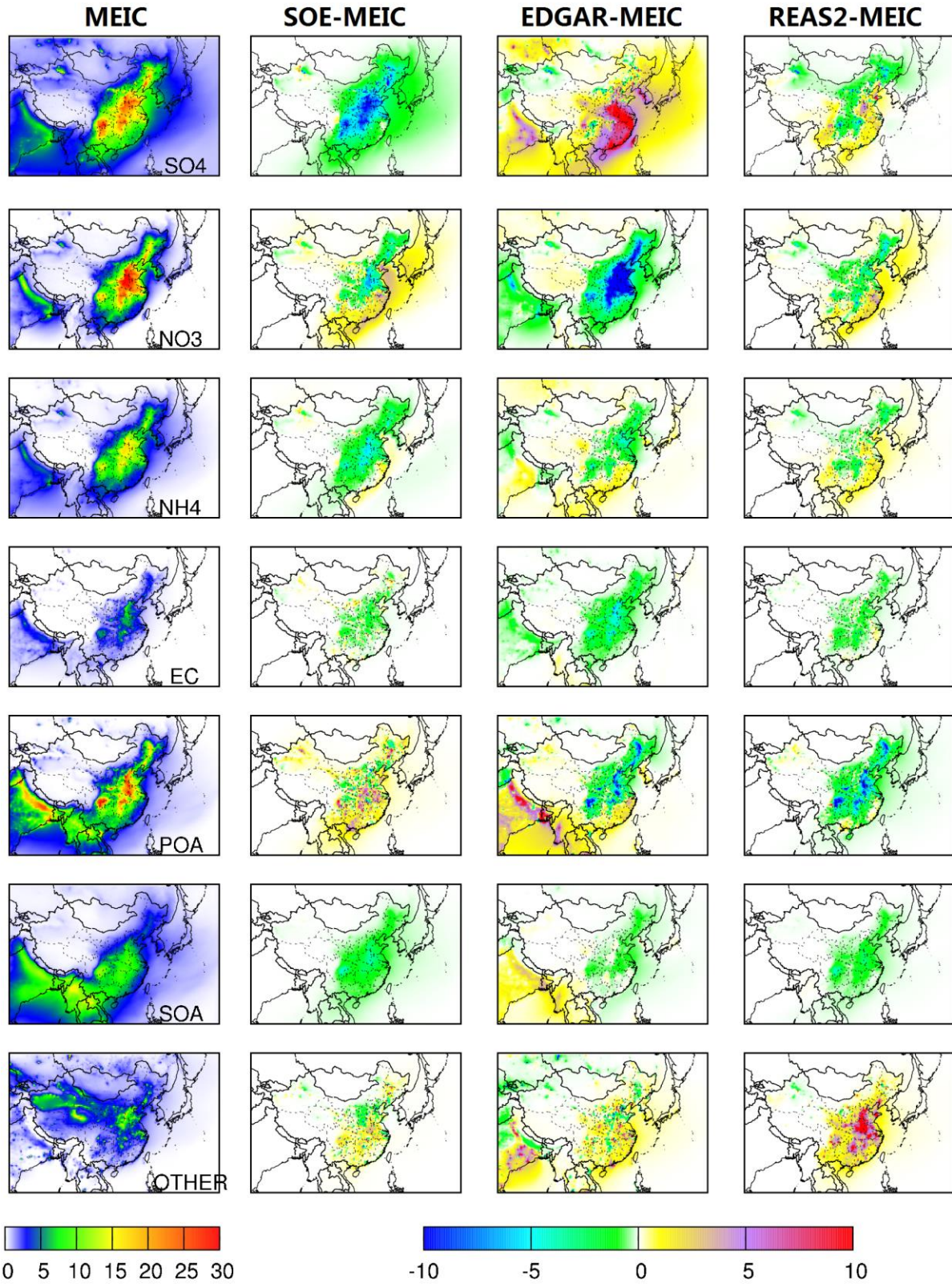


Figure 6. Spatial difference of model predicted annual $PM_{2.5}$ components (in the horizontal panels) with different inventories (in the vertical panels). Units are $\mu g m^{-3}$.

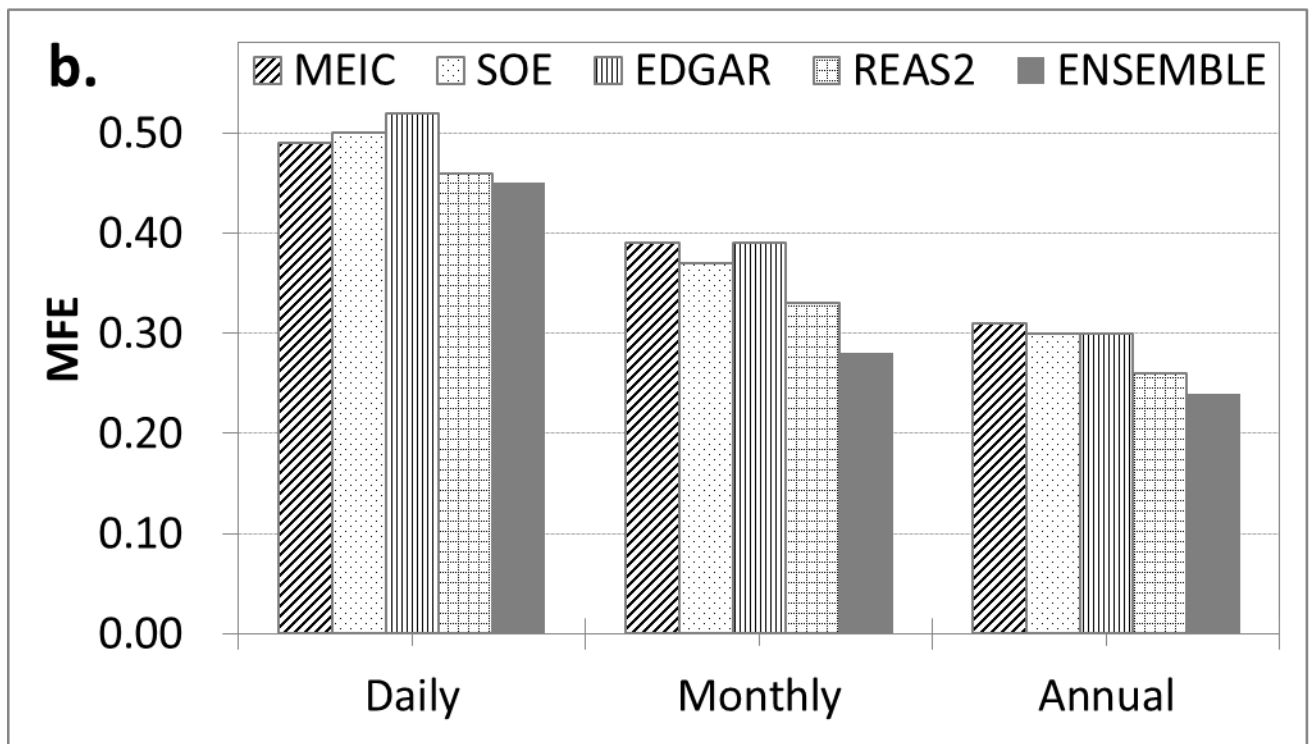
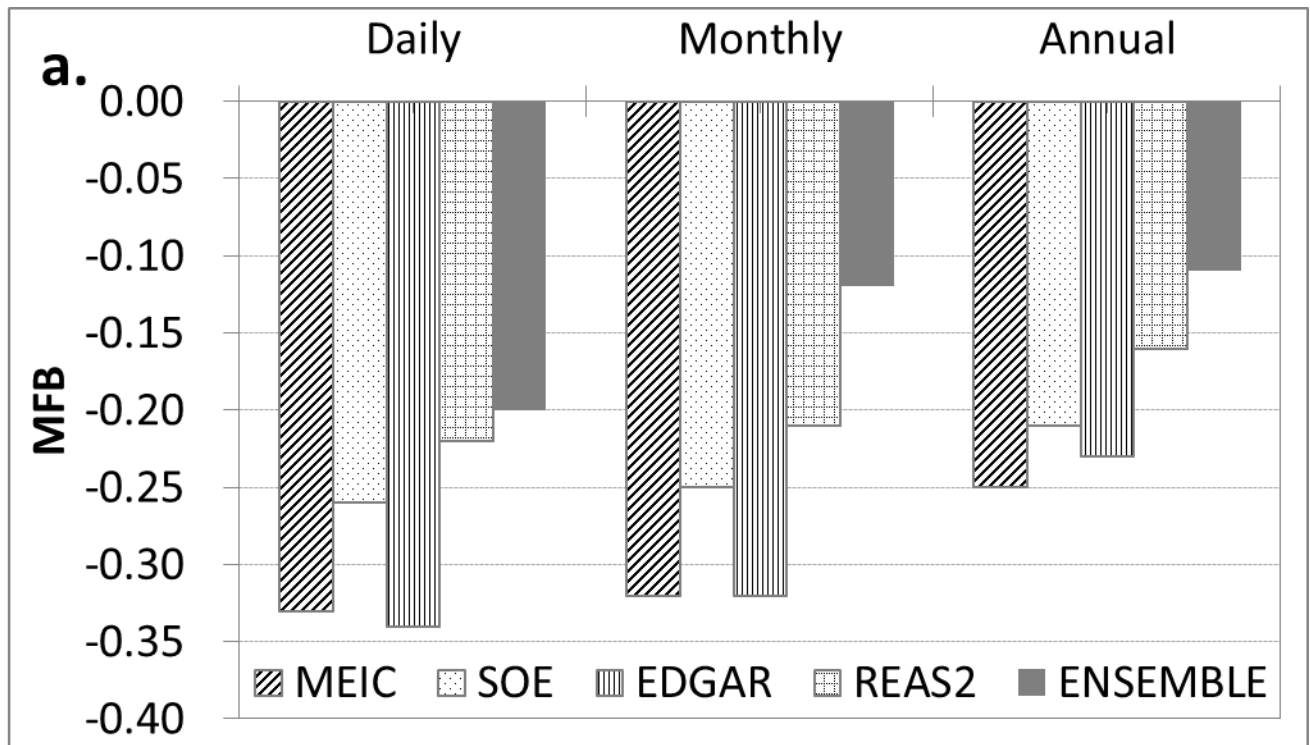


Figure 7. MFB and MFE of predicted $PM_{2.5}$ for with an averaging time of 24 hours, 1 month, and 1 year based on the individual inventories and the ensemble.

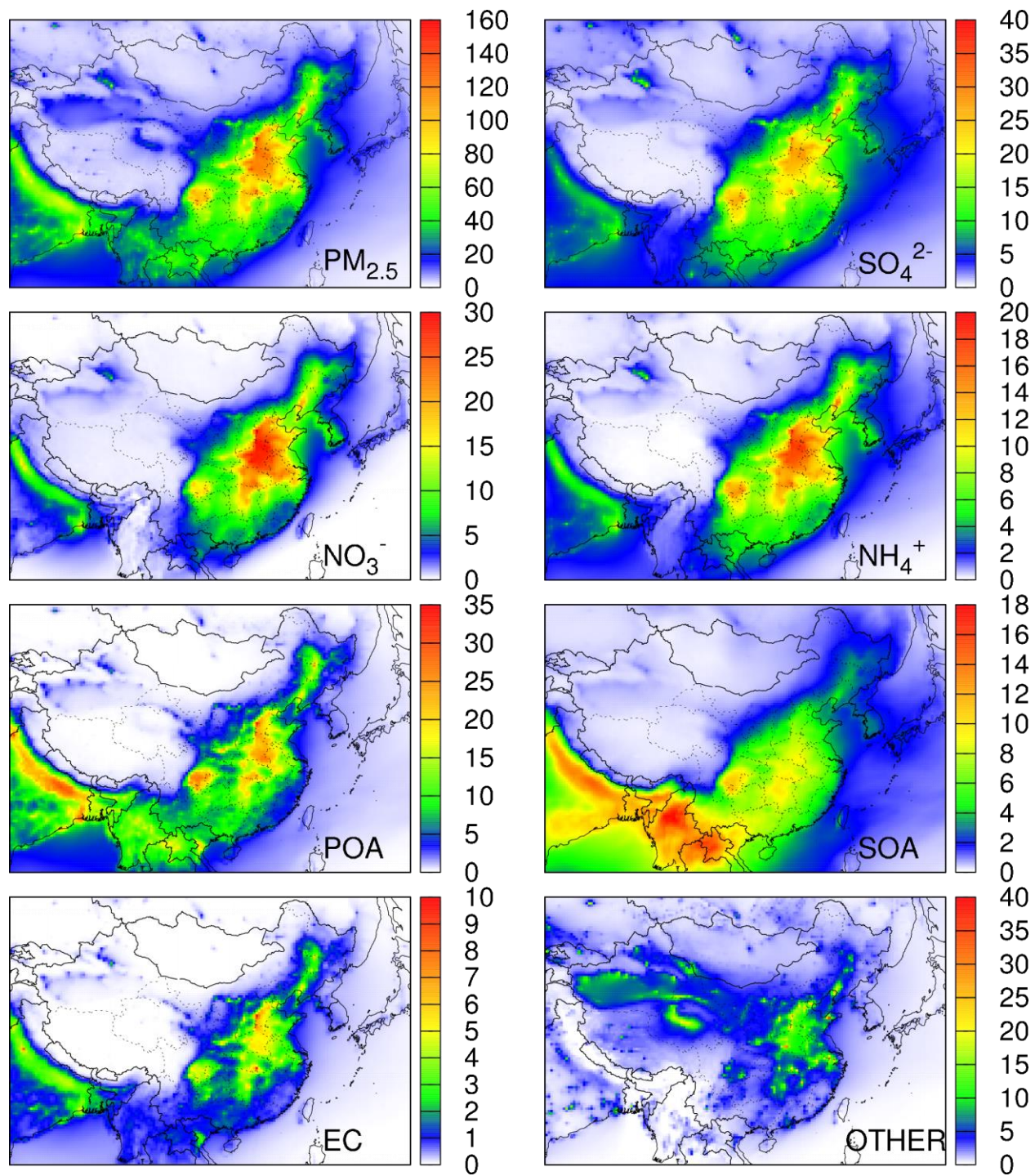


Figure 8. Spatial distributions of $\text{PM}_{2.5}$ and its components in the ensemble predictions. Units are $\mu\text{g m}^{-3}$. The scales of the panels are different. White indicates zero while blue, green, yellow and red means concentrations from low to high.